Aerosol Science & Technology

ISSN: 0278-6826 (Print) 1521-7388 (Online) Journal homepage: http://www.tandfonline.com/loi/uast20

A Numerical Investigation of Particle Deposition on a Square Cylinder Placed in a Channel Flow

D. J. Brandon & S. K. Aggarwal

Aerosol Science and Technology 34: 340–352 (2001)

Published by Taylor and Francis
0278-6826/01/$12.00 + .00

A Numerical Investigation of Particle Deposition on a Square Cylinder Placed in a Channel Flow

D. J. Brandon and S. K. Aggarwal
Department of Mechanical Engineering, University of Illinois at Chicago, Chicago, Illinois

Particle deposition on a square cylinder placed in a rectangular channel was investigated for unsteady vortical flows. For the two-phase flow simulations, the unsteady gas flow field was computed by solving the incompressible Navier-Stokes equations using a staggered-grid control volume approach and the Marker-and-Cell (MAC) technique. The particle dynamics were simulated using the modified Basset-Bousinesq-Oseen (BBO) equation. The gas-phase algorithm was validated using four test problems involving both steady and unsteady flows. Numerical experiments were also conducted to evaluate the relative contributions of various terms in the BBO equation. For particle dynamics in unsteady vortical flows, all the secondary terms were found to be negligible compared to the steady state viscous term at particle density ratios >20. The two-phase flow model and the detailed flow visualization were then employed to characterize particle dispersion and deposition as a function of the Reynolds number, particle Stokes number (St), and density ratio (ε). Particle dispersion in the cylinder wake exhibited a typical nonmonotonic behavior. Particles with St < 0.1 behaved like fluid particles, whereas those with St between 0.1 and 0.5 dispersed more than fluid particles and those with St > 1.0 were essentially unaffected by the flow in the near wake region. In addition, the small St particles were distributed in the vortex core, while the intermediate St particles were distributed around the vortex periphery. For $\varepsilon > 20$, the particle deposition was essentially characterized by the Stokes number. The amount of deposition increased precipitously as St was increased from zero to unity, then increased slowly for St between 1 to 3, and was essentially independent of St for St > 3.0. For the range of Reynolds numbers investigated, which included both laminar and transitional regimes, the Reynolds number (Re) had a negligible effect on particle deposition, but a more discernible effect on particle distribution and dispersion.

INTRODUCTION

The transport of particles in laminar and turbulent flows has numerous applications in engineering biological and environmental systems. The deposition of aerosol particles in channels and pipes, as well as in bends and contractions, is important in many applications, including dust inhalation and human respiratory systems, chip fabrication, particle size characterization, and sampling of radioactive aerosols. In coal combustion systems and coal liquefaction-gasification pipelines, the erosion of material by solid particle impact is an important problem. In order to gain a fundamental understanding of the particle impaction and deposition phenomena, as well as to make meaningful design improvements, it is essential to develop reliable predictive models for the transient two-phase flows encountered in these systems.

Early studies of particle-laden flows employed analytical and theoretical techniques to examine deposition and sedimentation processes in various systems. Bowen et al. (1976) used a theoretical approach to approximate the deposition of colloidal particles onto the walls of rectangular and cylindrical channels for fully developed laminar flows. Simons (1984) modeled the deposition and spatial distribution of aerosol particles inside an enclosed vessel under turbulent flow conditions. Gupta and Jackson (1985) examined surface deposition and fouling in conventional gas turbine combustion systems for hot gaseous turbulent flows. The effects of thermophoresis and eddy impaction on deposition efficiency were investigated.

Stratmann et al. (1988) numerically modeled the deposition of small particles onto a flat plate in a stagnation flow to mimic the contamination of wafer surfaces in the electronics industry. Duffy and Darby (1991) examined the surface structure of deposited material in turbulent gas flows. Other studies (Viatistas 1992; Vasak et al. 1995; Konstandopoulos and Rosner 1995a,b) investigated the phenomena of particle deposition on channel walls for a variety of flow conditions. For example, Vasak et al. (1995) used fine silica and polystyrene particles in a channel in which the particles and channel wall were given opposite charges.

In recent years, increasingly large numbers of numerical studies have focused on particle transport and deposition. Tu and Fletcher (1995) numerically investigated the erosive wear in a channel by examining the concentration of particles at a 90° bend. They observed an increase in particle concentration near the outer wall of the bend as the Stokes number is increased. Wang and Squires (1996) investigated the turbulent flow effects on particle deposition in a vertical channel flow using DNS and

Received 17August 1999; accepted 20 March 2000.
Address correspondence to S. K. Aggarwal, Department of Mechanical Engineering (M/C 251), University of Illinois at Chicago, 842 W. Taylor St., Chicago, IL 60607-7022. E-mail: ska@uic.edu

LES models. Barton (1995) simulated particle dynamics in a laminar flow over a backward facing step. Recent studies concerning deposition in practical systems include those dealing with aerosol sampling and transport systems (Chen and Pui 1995; Muyshondt et al. 1996), electrostatic precipitators (Suh and Kim 1996), and virtual impactors (Asgharian and Godo 1997). In this context, Ye and Pui (1997) reviewed studies dealing with particle deposition in abrupt contractions. Numerical investigations of the deposition of oral inhalants in the human respiratory system have also been reported (Yu et al. 1996; Zhang et al. 1997).

Several experimental (Longmire and Eaton 1992; Lazaro and Lasheras 1992) and numerical (Crowe et al. 1988; Uthuppan et al. 1994; Aggarwal 1994; Chang and Kailasanath 1996) studies have also examined the phenomena of particle dispersion in shear flows whose dynamics and mixing characteristics are dominated by large-scale vortex structures. The particle dispersion in such flows was found to be characterized by the Stokes number (St), defined as the ratio of a particle response time to a characteristic flow time. While the flow time was defined by the dominant frequency associated with the vortex structures, the particle response time was defined as $t_p = \rho_p d_p^2/18\mu$, based on the steady-state Stokes drag law. Here, ρ_p is the particle density, d_p the particle diameter, and μ the gas viscosity. Both experimental and numerical studies have shown that the presence of large vortex structures lead to a size-selective dispersion behavior such that the particles with Stokes number near unity (St $\sim$ 1.0) exhibit the maximum dispersion. Whereas small particles (small Stokes number) get caught in the vortical structures and large particles (large Stokes number) pass through them, the intermediate size particles (St $\sim$ 1.0) get trapped in the vortex structures and are then flung out of them.

The objective of the present study is to numerically simulate and analyze particle transport and deposition in an unsteady particle laden flow over a square cylinder placed in a channel. The presence of the cylinder (bluff body) creates an unsteady or periodic flow field characterized by the presence of shedding vortices and recirculation in the wake region of the cylinder. In addition, the flow contains a stagnation region in front of the cylinder, as well as regions of flow acceleration and deceleration around it. The particles injected in such complex, transient flows are subjected to both steady and unsteady lift and drag forces, caused by the effects of flow nonuniformity (shear), pressure gradient, and unsteady relative acceleration. In order to account for these effects, the particle dynamics are simulated by using the modified Basset-Bousinesq-Oseen (BBO) equation (Barton 1995; Maxey and Riley 1983; Peng and Aggarwal 1995), which is further modified to include the large Reynolds number effects. A detailed two-phase simulation model and flow visualization are employed to analyze the transient flow field and vortex dynamics, as well as the particle dynamics and dispersion behavior. Numerical experiments are performed to characterize particle deposition as a function of the Stokes number, Reynolds number, ratio of particle density to gas density, and other parameters. The relative contributions of various force terms in the BBO equation are also quantified.

Although previous investigations have examined particle deposition in different flow configurations, we are not aware of any publication dealing with the deposition of solid particles on bluff bodies in unsteady particle-laden flows. Most previous studies have examined particulate deposition onto internal walls, such as pipes, channels, and arteries, while others have examined their transport in unconfined flows. Recently, Thatcher and Nazaroff (1997) investigated the effect of small-scale obstructions on particle deposition in a natural convection flow, while Bakkom et al. (1996) numerically simulated the effects of particle-fluid coupling on bluff body wakes using evaporative droplets. However, the aspects dealing with particle deposition on a bluff body were not examined.

THE PHYSICAL-NUMERICAL MODEL

The physical system considers a particle-laden flow over a bluff body placed in a rectangular channel of width H and length L. The bluff body represented by a square cylinder, with each side of length B, is located along the channel centerline. Figure 1 shows a schematic of the channel and the distribution of grid

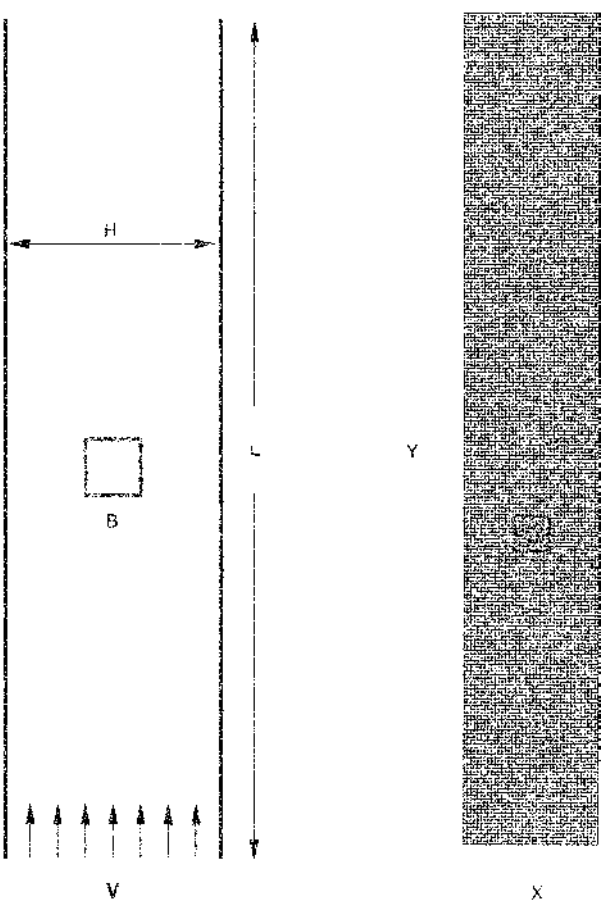

Figure 1. Schematic of rectangular channel and square cylinder.

points within the computational domain. The channel width is $4B$ and the length (L) is $24B$. Particles are injected from several locations upstream of the cylinder.

Gas-Phase Equations

The equations governing the unsteady incompressible gas flow are the continuity and Navier-Stokes equations, which can be written in the nondimensional form as

$$\frac{\partial u}{\partial x} + \frac{\partial v}{\partial y} = 0, \quad [1]$$

$$\frac{\partial u}{\partial t} + u\frac{\partial u}{\partial x} + v\frac{\partial u}{\partial y} = -\frac{\partial p}{\partial x} + \frac{1}{\mathrm{Re}}\left\{\frac{\partial^2 u}{\partial x^2} + \frac{\partial^2 u}{\partial y^2}\right\}, \quad [2]$$

$$\frac{\partial v}{\partial t} + u\frac{\partial v}{\partial x} + v\frac{\partial v}{\partial y} = -\frac{\partial p}{\partial y} + Fr^{-2} + \frac{1}{\mathrm{Re}}\left\{\frac{\partial^2 v}{\partial x^2} + \frac{\partial^2 v}{\partial y^2}\right\}. \quad [3]$$

Here Re and Fr are the Reynolds and Froude numbers defined, respectively, as $\mathrm{Re} = BV_0/v$ and $Fr = V_0/\sqrt{gB}$, where g is the gravitational acceleration and V_0 the velocity at the channel entrance. The equations are normalized by using B as the length scale, V_0 as the velocity scale, and B/V_0 as the time scale.

The equations are descretized by using a control-volume approach with a staggered grid system (Hirt et al. 1975; Harlow and Welch 1965). The numerical solution employs the marker-and-cell (MAC) methodology developed by Hirt et al. (1975) and Harlow and Welch (1965). The physical and computational domains of the channel and cylinder are illustrated in Figure 1. The cylinder is centrally located $8.5B$ downstream of the channel inlet, and a uniform inlet flow condition is prescribed at the channel entrance. At the channel exit, a continuous outflow condition is prescribed by setting $\partial u/\partial y = \partial v/\partial y = 0$. On the left and right walls, as well as on the square cylinder boundaries, no-slip boundary conditions are prescribed. The boundary conditions are implemented by using rows or columns of fictitious cells as appropriate. Additional details are provided in Hirt et al. (1975), Harlow and Welch (1965), and Brandon (1999).

Particle Dynamics Equations

As noted earlier, particles under consideration traverse a complex transient flow field containing regions of stagnation flow, separating flow, recirculation, and vortex structures. Consequently, a detailed particle dynamics model based on the modified BBO equation (Maxey and Riley 1983; Peng and Aggarwal 1995) is developed to calculate their trajectories. The BBO equation is further modified to account for the high Reynolds number effects. The nondimensional form of this equation can be written as

$$\begin{aligned}\frac{du_{pi}}{dt} = {} & C_{Ds}\frac{u_i - u_{pi}}{St} + \frac{1}{\varepsilon}\frac{Du_i}{Dt} + C_A\frac{1}{2}\frac{1}{\varepsilon}\frac{d}{dt}(u_i - u_{pi}) \\ & + \frac{1.2C_H}{(\varepsilon St)^{1/2}}\int_{t_0}^{t}\frac{d(u_i - u_{pi})/dt}{\sqrt{t - t^*}}dt^* \\ & + \frac{0.47}{(\varepsilon St)^{1/2}}\frac{d_{ij}(u_i - u_{pi})}{(d_{lk}d_{kl})^{1/4}} + \left(1 - \frac{1}{\varepsilon}\right)Fr^{-2}. \quad [4]\end{aligned}$$

The equation is written in a vector form where u_i and u_{pi} represent, respectively, the gas and particle velocity vectors. The instantaneous particle location $x_i(t)$ is obtained from

$$\frac{dx_i}{dt} = u_{pi}. \quad [5]$$

Equations (4) and (5) are normalized using B and V_0 as the length and velocity scales, respectively. The terms on the right-hand side of Equation (4) represent, respectively, the steady state drag, pressure drag, virtual or added mass effect, Basset history term, Saffman lift term, and gravity term. More detailed discussion of these terms can be found in Barton (1995), Maxey and Riley (1983), and Peng and Aggarwal (1995).

The nondimensional BBO equation (4) highlights two key parameters, namely, the Stokes number (St) and the density ratio (ε). The density ratio represents the ratio of particle density (ρ_p) to gas density (ρ). The Stokes number is defined as the ratio of particle response time (t_p) to a characteristic flow time (t_f) and can be written as

$$\mathrm{St} = \frac{t_p}{t_f} = \frac{d_p^2\varepsilon\mathrm{Re}}{18B^2}, \quad [6]$$

where d_p is the particle diameter. C_{Ds} in Equation (4) is a correction factor that accounts for the high Reynolds number effect on the steady state drag coefficient and is given by

$$C_{Ds} = 1 + \frac{\mathrm{Re}_p^{2/3}}{6}. \quad [7]$$

The particle Reynolds number is defined as $\mathrm{Re}_p = v_r d_p \rho/\mu$, where v_r is the magnitude of relative particle velocity. Further, C_A and C_H in Equation (4) are the correction factors accounting for the high Reynolds number effects in the added mass and Basset history terms. Following Odar and Hamilton (1964), C_A and C_H are expressed as

$$C_A = 1.05 - \frac{0.066}{A_c^2 + 0.12} \quad \text{and} \quad C_H = 2.88 + \frac{3.12}{(1 + A_c)^3}, \quad [8]$$

where A_c is the relative acceleration factor defined as

$$A_C = \frac{v_r^2/d_p}{dv_r/dt}. \quad [9]$$

Finally, d_{ij} in the Saffman lift term is the deformation rate tensor defined as

$$d_{ij} = \frac{1}{2}(u_{ij} + u_{ji}) \quad \text{with} \quad u_{ij} = \frac{\partial u_i}{\partial x_j}. \quad [10]$$

Particles of given velocity and Stokes number are injected at specified locations upstream of the cylinder. Their trajectories are computed by solving Equations (4) and (5) using a fourth-order Runge-Kutta numerical method (Jaluria 1988). Since the

instantaneous particle locations do not coincide with the gas-phase grid points, a second-order interpolation is employed to obtain the gas velocity at the particle locations. The particle deposition on the cylinder is assumed to occur when its instantaneous location is within one particle radius from the cylinder surface. Once the particle is deposited on the cylinder surface, its trajectory is no longer calculated. This implies the assumption that the particle is captured by the surface.

RESULTS AND DISCUSSION

Results on Code Validation

Numerical experiments were performed to validate the computational algorithm. Test cases included a driven cavity flow, transient flow in a cavity induced by an oscillating lid, developing flow in a channel, and unsteady flow over a square cylinder. Some representative results are depicted in Figures 2–4. Figure 2 presents a comparison between our numerical results and those of Peyret and Taylor (1983) and Ghia et al. (1982) for a driven cavity flow. The axial velocity at the midplane of the cavity is plotted as a function of the transverse coordinate. There is excellent agreement between the four sets of results shown in Figure 2. Results of code validation for a transient flow are presented in Figure 3, which shows the plot of $C_D \cdot \mathrm{Re}$ versus the nondimensional time for an impulsively started flow in a square cavity. Here C_D and Re are the drag coefficient and Reynolds number, respectively (Soh and Goodrich 1988). These results are in good agreement with those reported by Soh and Goodrich (1988). Figure 4 shows the variation of $C_f \cdot \mathrm{Re}$ along the channel wall for the developing channel flow at four different Reynolds

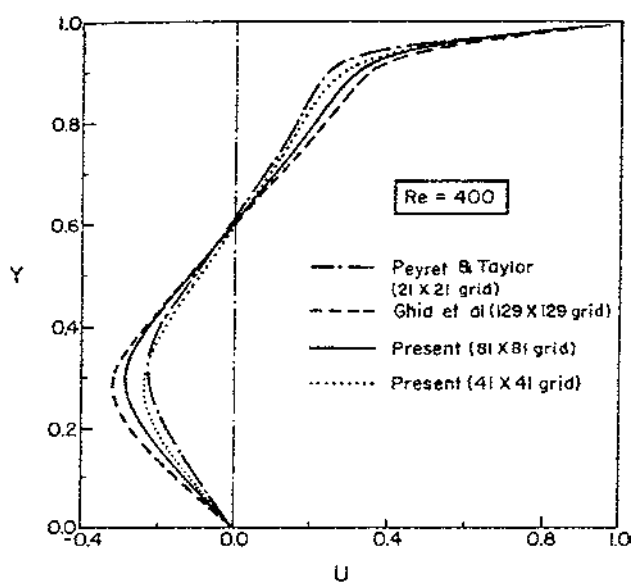

Figure 2. Variation of U-velocity at the midplane of a lid-driven square cavity flow. Comparison of numerical results (obtained with two different grid densities) with those of Peyret and Taylor (1983) and Ghia et al. (1982).

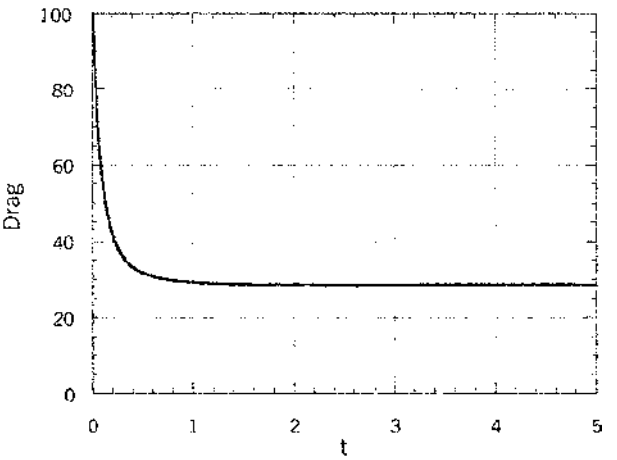

Figure 3. Plot of nondimensional drag (C_D Re) versus nondimensional time t for an impulsively started flow in a square cavity (Re = 400, $\Delta t = 0.01$).

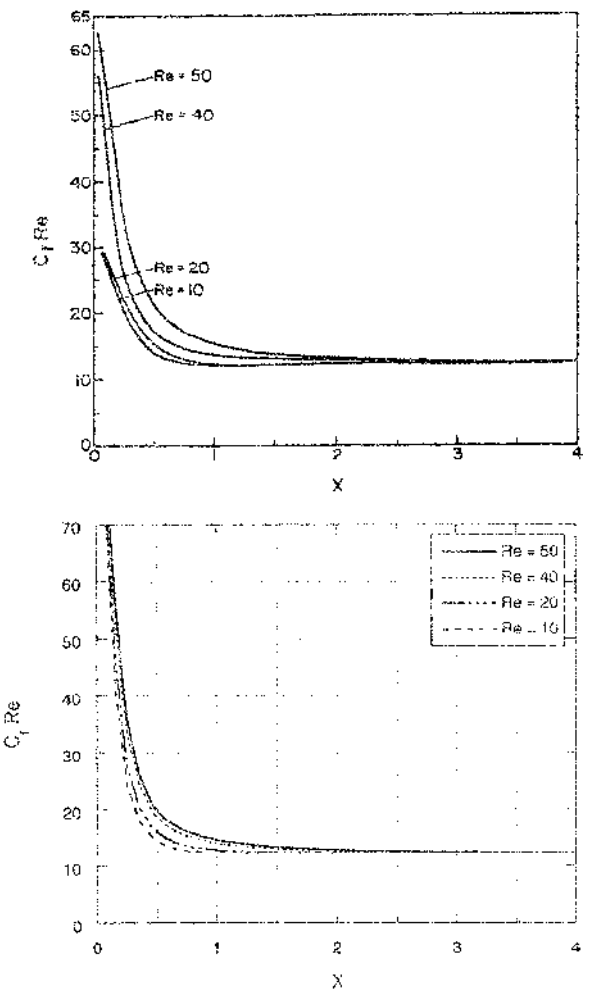

Figure 4. Variation of C_f Re along the channel wall for several Reynolds numbers: (a) from Mukhopadhyay et al. (1993); (b) presents results.

numbers. Here C_f represents the standard friction coefficient for a channel flow (Mukhopadhyay et al. 1993). Again, there is a good agreement between our results (cf. Figure 4b) and those of Mukhopadhyay et al. (1993). More detailed results for the above three cases are provided in Brandon (1999).

Code Validation for Flow over a Cylinder

As a final validation, we present numerical results for flow over a square cylinder. A schematic of the model domain is depicted in Figure 1. For low to moderate Reynolds numbers, the flow is characterized by periodic asymmetric shedding of vortices in the aft of the cylinder. An instantaneous image of the transient flow field at Re = 1000 computed by using the gas-phase code is presented in Figure 5. The velocity vector and stream-trace plots are shown in Figures 5a and 5b, respectively. These plots clearly depict the regions of stagnating flow, flow separation along the top ($x = 0.5$) and bottom ($x = -0.5$) walls of the cylinder, and asymmetric vortex shedding in the cylinder wake. Also depicted are the Von-Karman vortex sheet and the unsteady wake structure (Davis et al. 1984). Further downstream in the wake, the flow unsteadiness is dampened by the channel walls. Given a sufficiently long channel, the velocity distribution would eventually return to a fully-developed parabolic profile.

The asymmetric periodic vortex shedding is depicted more clearly in Figure 6, which contains six instantaneous images of the flow field during one vortex period. The image at $t = 0$ shows a vortex in the process of being shed from the top wall (at $t = 2.0$). As this vortex grows in size and convects downstream, another vortex begins to roll up near the bottom wall. As the bottom vortex forms and moves downstream ($t = 3.0$ and 4.0), another one starts forming at the top wall ($t = 5.0$) and the process repeats itself. The nondimensional shedding frequency or the Strouhal number, $S = f \cdot B/Vo$, where f is the shedding frequency in Hz, was computed by taking the fast Fourier transform (FFT) of the velocity history recorded at selected spatial locations in the cylinder wake. The velocity data was recorded over seventeen vortex periods. The computed Strouhal numbers for three different mesh densities and those reported by Mukhopadhyay et al. (1993) are given in Table 1. The important observation is that the 40 × 240 grid yields results that are nearly grid independent and in agreement with those reported by Mukhopadhyay et al. (1993).

Numerical experiments were also performed to obtain the dependence of Strouhal number on the Reynolds number and blockage ratio. These results are summarized in Table 2. The Strouhal number exhibits relatively strong dependence on the blockage ratio, increasing from 0.22 to 0.27 as B/H is increased from 0.25 to 0.33, but weak dependence on the Reynolds number, decreasing from 0.22 to 0.195 as Re is increased from 250 to 2000. These results are in accord with those given in Davis et al. (1984) and Mukhopadhyay et al. (1993).

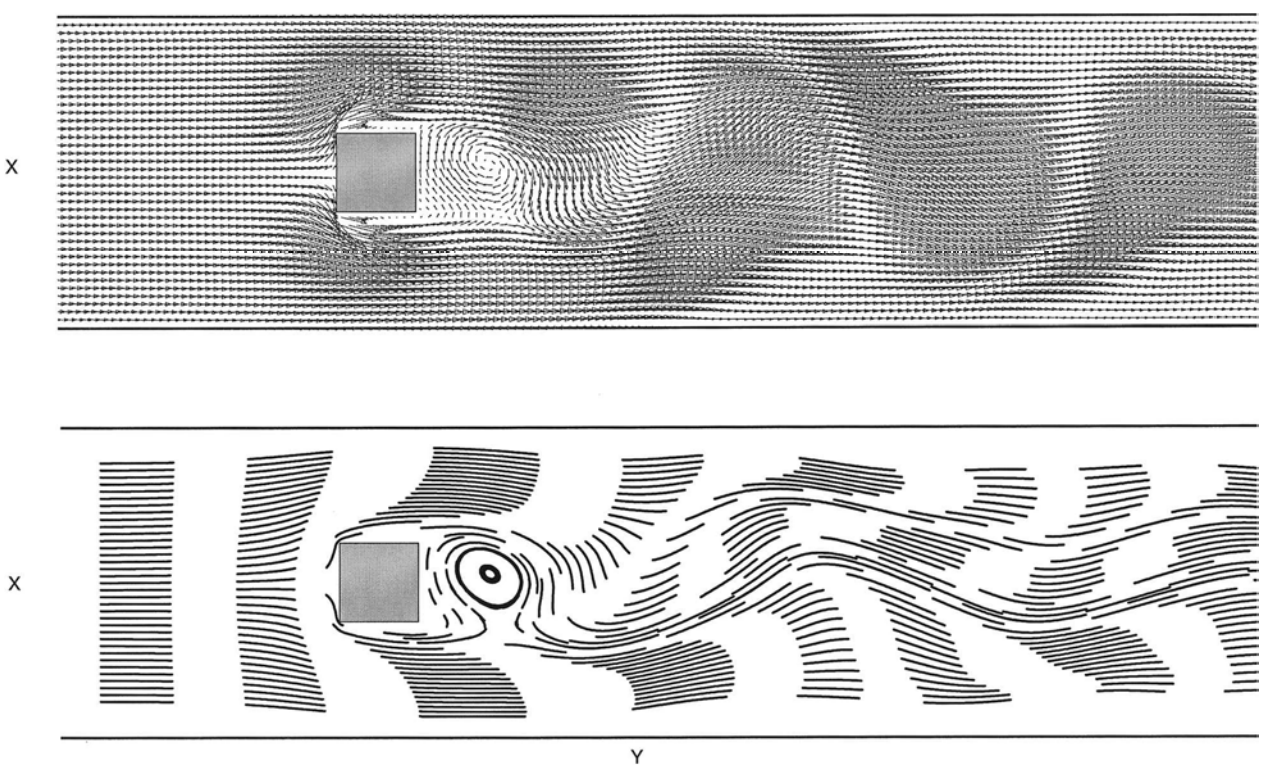

Figure 5. Instantaneous image of the unsteady flow field showing periodic, asymmetric vortex shedding: (a) velocity vector plot; (b) stream-trace plot. The Reynolds number is 1000.

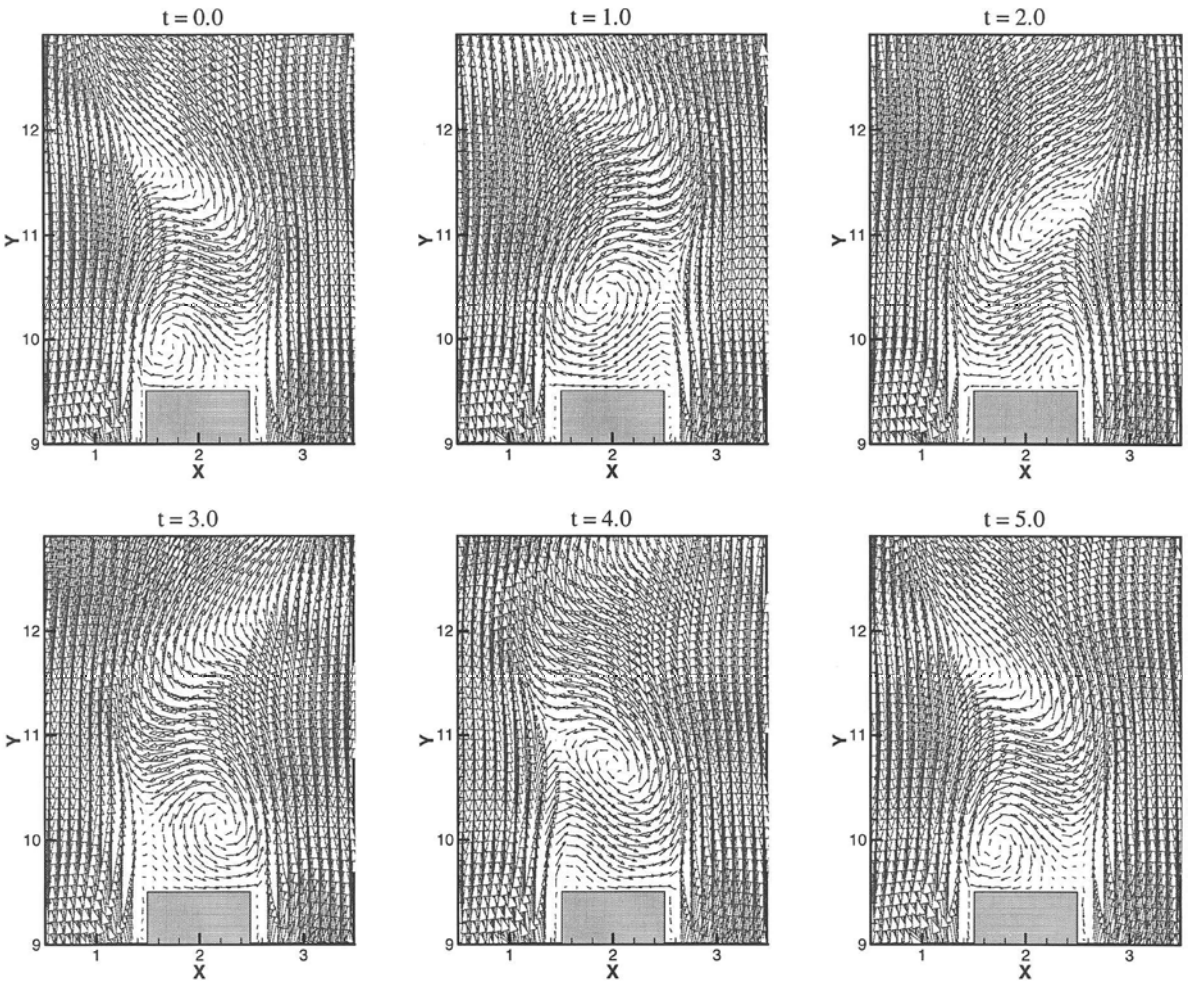

Figure 6. Instantaneous images of the flow field in terms of velocity vector plots during one vortex time. The Reynolds number is 1000.

Particle Dynamics

The modified BBO equation (4) has been a subject of extensive research. While many investigators (Barton 1995; Lazaro and Lasheras 1992; Peng and Aggarwal 1995) have examined the relative magnitude of various force terms in the equation, others have focused on modifying these terms under specific conditions. It has often been suggested (Peng and Aggarwal 1995) that for large density ratios ($\varepsilon \gg 1$), terms representing the pressure drag, virtual mass, Basset history, and Saffman lift are negligible compared to the steady state viscous drag. However, several studies (Peng and Aggarwal 1995; Odar and Hamilton 1964) have found that under specific conditions the

Table 1
Strouhal numbers for different size meshes

Grid	Re	$\frac{B}{H}$	Strouhal number (S)
32 × 96	250	0.25	0.183
40 × 240	250	0.25	0.220
64 × 240	250	0.25	0.220
*34 × 200	250	0.25	0.212

*From Mukhopadhyay et al. (1993).

Table 2
Strouhal numbers for different Reynolds numbers and blockage ratios

Re	$\frac{B}{H}$	Strouhal number (S)
200	0.25	0.2197
250	0.25	0.2197
500	0.25	0.2075
750	0.25	0.2075
1000	0.25	0.1953
1500	0.25	0.1953
2000	0.25	0.1953
250	0.33	0.2686

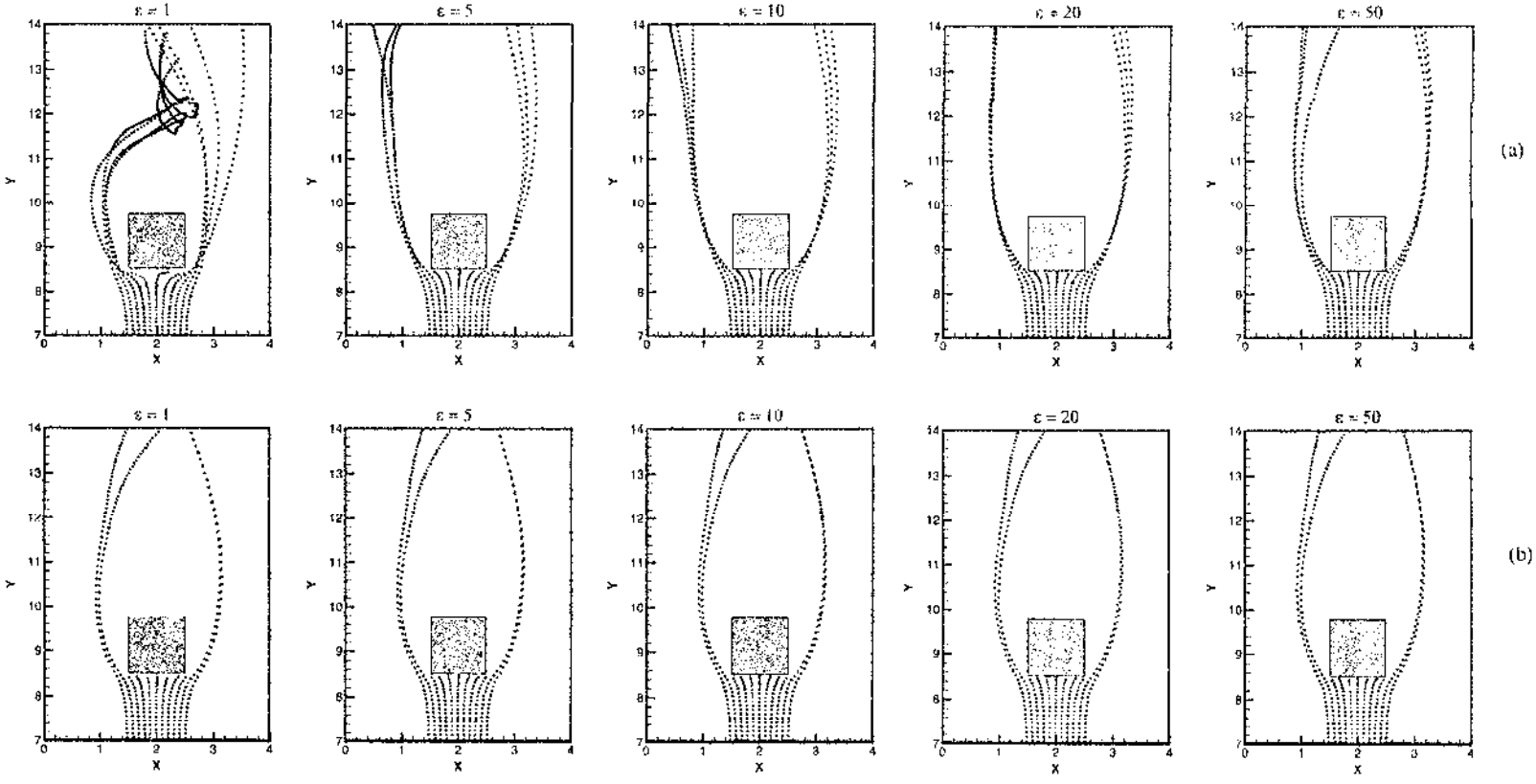

Figure 7. Particle trajectories for different density ratios (Re = 1000, St = 1): (a) using all the terms in the BBO equation (4); (b) using only the steady state viscous drag term.

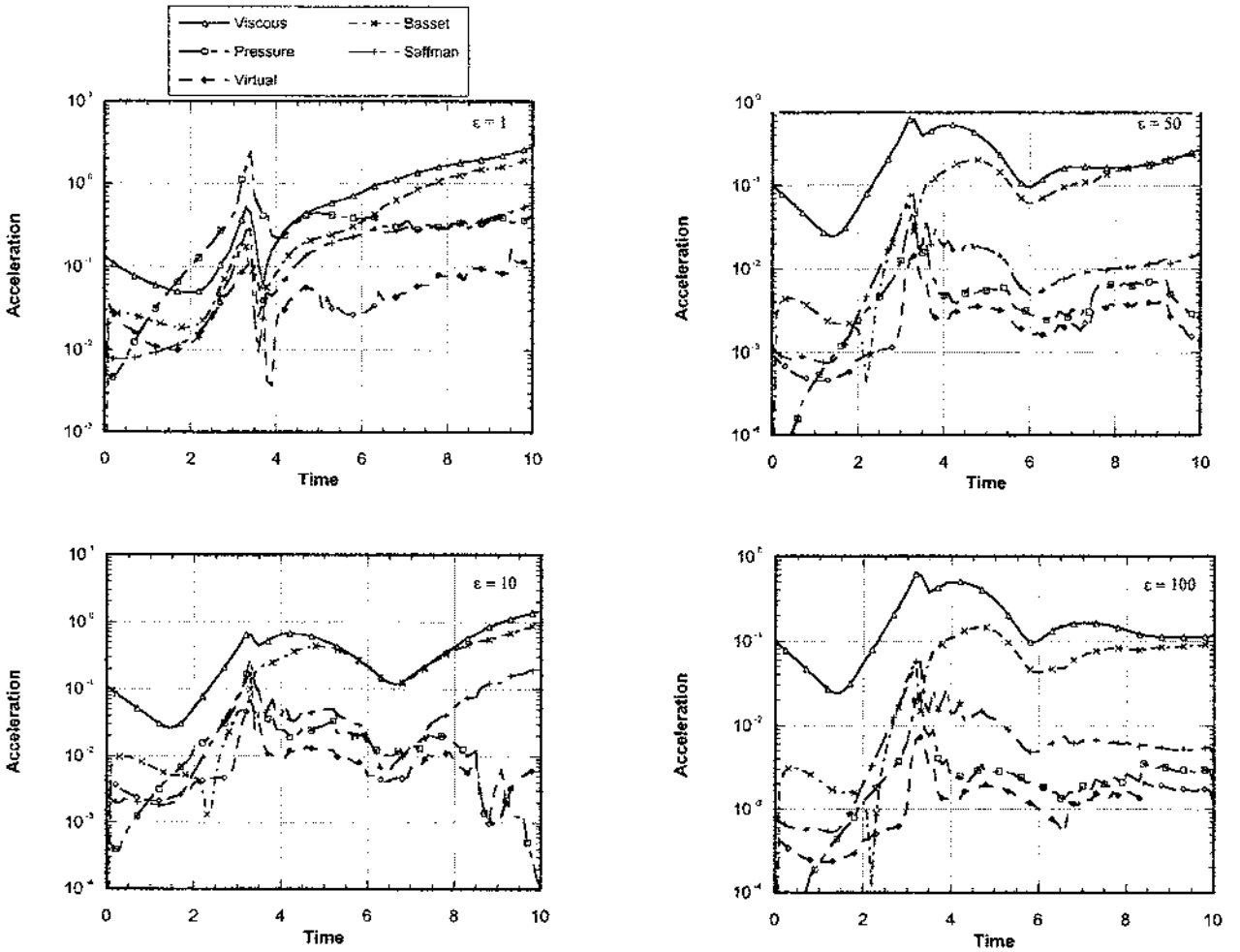

Figure 8. Temporal history of various force terms in Equation (4) for different density ratios, Re = 1000, St = 1.0.

effects of flow nonuniformity and particle relative acceleration may be important even when the particle density is much higher than the gas density.

In the present study, we investigated this aspect by analyzing particle dynamics in an unsteady vortical flow generated by the presence of a square cylinder. Particles with prescribed Stokes number and velocity were injected at locations upstream of the cylinder and their trajectories were calculated for different density ratios (ε). A qualitative evaluation of the viscous drag term relative to all the other terms in the BBO equation (4) is presented in Figure 7, which shows the trajectories of eleven particles for $\varepsilon = 1$, 5, 10, 20, and 50. Two cases are considered. In the first case, trajectories are computed using all the terms in Equation (4), whereas in the second, trajectories are calculated using only the steady state viscous drag (or the first term). The Reynolds number is 1000 and the particle Stokes number is 1.0. The effects of these two parameters are analyzed in the next section. Results indicate that for $\varepsilon < 20$, the particle trajectory and deposition exhibit notable differences between the two cases and therefore are sensitive to the density ratio. However, for $\varepsilon \geq 20$, the differences become negligible and the particle dynamics and deposition become essentially independent of ε for a fixed Stokes number.

A quantitative comparison of various force terms of Equation (4) is presented in Figure 8, which shows the temporal history of each term for different density ratios. The comparison again indicates that the contributions of all the nonviscous terms are nearly negligible for $\varepsilon \geq 20$, but become progressively important and comparable to that of the viscous term as ε is reduced below 10. Amongst various nonviscous terms, the Basset history term has the largest amplitude, followed by the Saffman lift term. An important implication therefore is that for the unsteady vortical flow investigated in the present study, the particle dynamics and deposition can be simulated by considering only the steady state viscous drag term in the BBO equation for $\varepsilon \geq 20$.

Particle Deposition

Results are now presented to characterize the effects of Reynolds number and Stokes number on particle distribution and deposition in the unsteady flow over a cylinder. First, the

unsteady flow over a cylinder placed in a channel is simulated by solving the gas-phase equations. Once the effect of starting transient becomes negligible and the flow exhibits periodic behavior, particles of given Stokes number and velocity are injected from several transverse locations $3.5B$ upstream of the cylinder. The time at which the particle injection starts is conveniently assigned a value $t = 0$. Twenty-one particles (one from each location) are injected every 0.2 s, which corresponds to about 525 particles during one vortex period. The particles' trajectories are computed by solving Equations (4) and (5).

The qualitative deposition behavior as a function of the particle Stokes number is depicted in Figure 9, which shows instantaneous images of the particles injected from 21 locations upstream of the cylinder. Each instantaneous image in Figure 9 for a given Stokes number contains about 3150 particles. The case $\mathrm{St} = 0$ corresponds, to the fluid or tracer particles. The flow Reynolds number is $\mathrm{Re} = 1000$, and the density ratio is $\varepsilon = 1000$. As discussed in the preceding section, for $\varepsilon = 1000$ the magnitude of all the secondary terms in Equation (4) is negligible compared to that of the steady state viscous term. Consequently, the trajectories are computed by using only the steady state viscous term.

The particle distribution in Figure 9 exhibits a typical nonmonotonic dispersion behavior. Particles with $\mathrm{St} < 0.1$ behave like fluid particles, whereas those with Stokes number in the range $0.1 < \mathrm{St} < 0.5$ exhibit intermediate St behavior, i.e., they are dispersed more than the fluid particles. On the other hand, particles with $\mathrm{St} > 1.0$ exhibit large St behavior, i.e., they are essentially unaffected by the flow in the near wake region. In addition, while the majority of small St particles are distributed in the core of each vortex, the majority of intermediate St particles are distributed around the vortex periphery. These observations regarding particle distribution and dispersion in the presence of large vortex structures are in accord with those reported by many experimental and numerical studies (Longmire and Eaton 1992; Lazaro and Lasheras 1992; Crowe et al. 1988; Uthuppan et al. 1994; Aggarwal 1994; Chang and Kailasanath 1996) dealing with particle dispersion in shear flows.

The above observations remain qualitatively similar as the Reynolds number is varied in the range $200 < \mathrm{Re} < 2000$. Within this range, as Re increases the size of vortex structures in the transverse direction become larger and, consequently, the particle dispersion increases. This is illustrated in Figure 10, where we plot the instantaneous particle distribution for two different Reynolds number, i.e., $\mathrm{Re} = 250$ and 1000. The Stokes number is 0.3. For a Reynolds number below 200, the flow becomes steady and vortex shedding is not observed, which is perhaps caused by the dissipative effect of the channel walls. For a Reynolds number above 2000, the flow tends to become turbulent.

The instantaneous images in Figure 9 also indicate that as the Stokes number is increased, the number of particles captured by the cylinder increases. More quantitative results concerning particle deposition are obtained by counting the number of particles captured by the cylinder compared to the total number of particles injected. Figure 11 shows the variation of the percent particle deposition as a function of the Stokes number for two different Reynolds numbers. The percent particle deposition is defined as

$$\eta = \frac{\textit{Particles deposited on cylinder surface}}{\textit{Particles injected into the flow}} \times 100. \qquad [11]$$

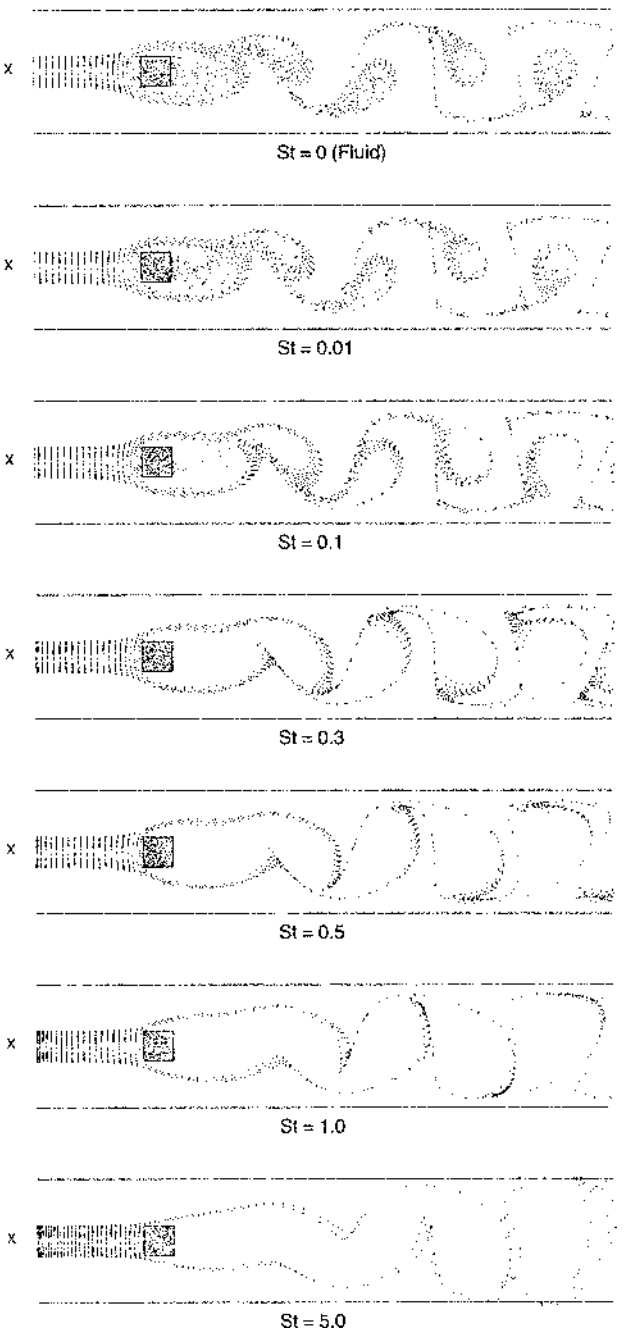

Figure 9. Instantaneous images of particles injected at 21 locations upstream of the cylinder for different Stokes number. The density ratio $\varepsilon = 1000$, and the flow Reynolds number $\mathrm{Re} = 1000$. For visual clarity, only half of the particles are shown.

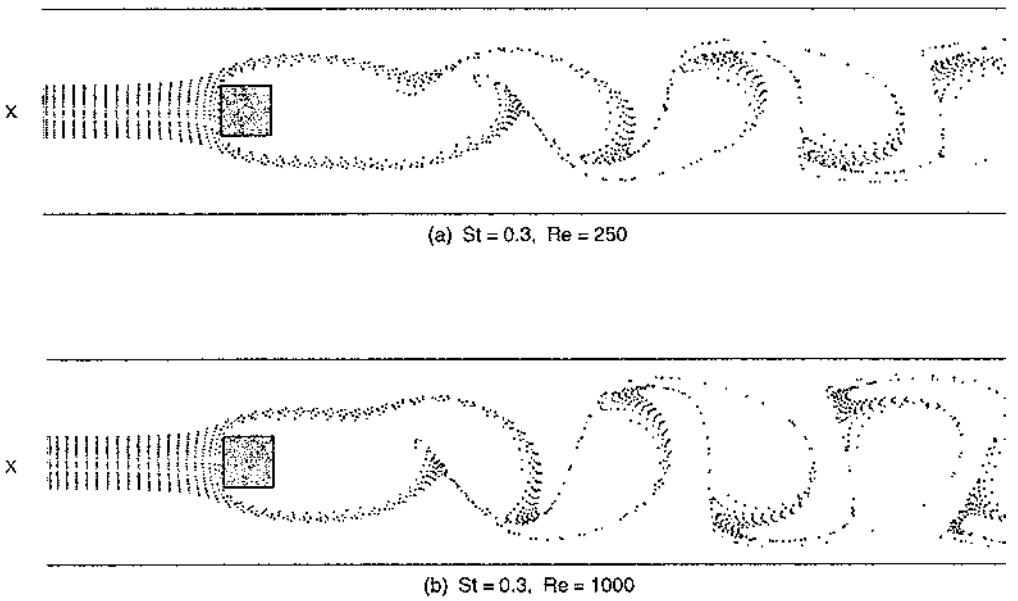

Figure 10. Instantaneous particle distribution for St = 0.3 and Re = 250 and 1000. Other conditions are the same as those in Figure 9.

Figure 11 indicates that the particle deposition depends strongly on the Stokes number, but is independent of the Reynolds number. The particle deposition first increases rapidly with St for St <1.0, then increases at a relatively slower rate for St between 1.0 and 3.0. For St >3.0, the particle deposition becomes essentially independent of St. These observations regarding particle deposition as a function of Stokes number are also captured qualitatively by the particle trajectory plots shown in Figure 12. It is important to note the difference between Figures 9 and 12. Figure 9 depicts instantaneous images of particles at $t = 31$ (counting from the instant the particle injection is started) for different Stokes numbers, whereas Figure 12 shows the trajectories of 11 particles over the entire time period from $t = 0$ to $t = 31$. Both the figures clearly show the strong dependence of the particle dynamics, distribution, and dispersion on the Stokes number.

Additional numerical experiments were performed to establish that the numerical results concerning particle deposition are independent of the total number of particles injected, the number of injection locations, and the temporal step size used in the computation. For the values of parameters used, the results were found to be independent of these parameters.

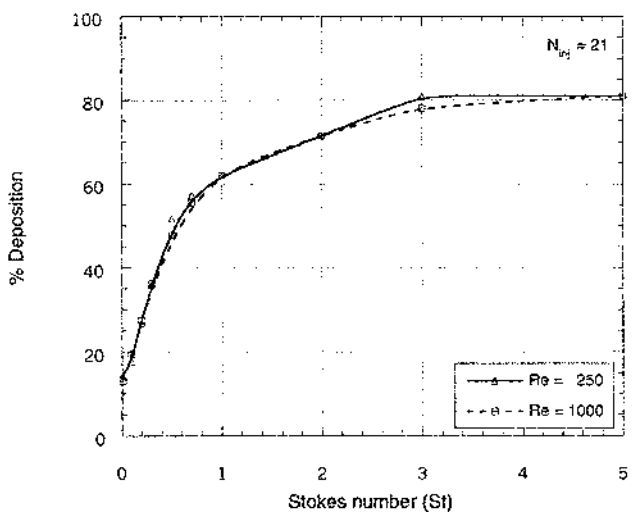

Figure 11. Variation of particle deposition with Stokes numbers for two different Reynolds numbers. Other conditions are the same as those in Figure 9.

CONCLUSIONS

In the present study, the particle dynamics in an unsteady vortical flow over a square cylinder placed in a channel was investigated. The range of Reynolds number considered included both the laminar and transitional regimes. The unsteady gas flow over a square cylinder was simulated by solving the incompressible Navier-Stokes equations using a direct numerical approach. The particle dynamics were simulated using the modified BBO equation that is further modified for the high Reynolds number effects.

The gas-phase numerical algorithm was first validated using several test problems involving both steady and unsteady flows. These included driven cavity flows, developing flow in a rectangular channel, and an unsteady flow over a square cylinder. For all the cases, the computed results were shown to be in good agreement with those reported by previous experimental and numerical studies. Detailed numerical experiments were also performed to evaluate the contribution of various force terms in the modified BBO equation. The two-phase flow model along

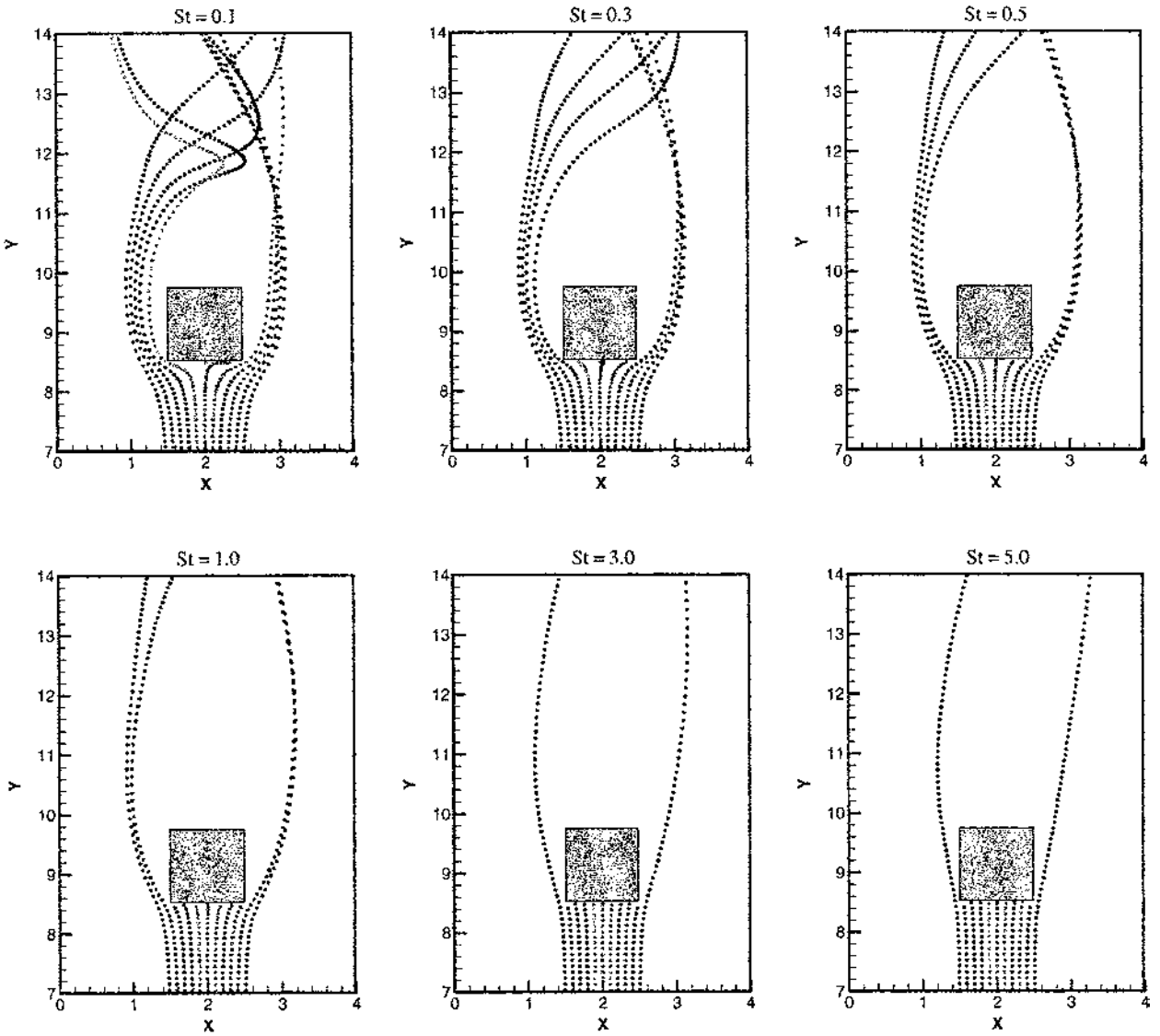

Figure 12. Particles' trajectories for different Stokes numbers. Other conditions are the same as those in Figure 9.

with detailed flow visualization were then employed to characterize particle dispersion and deposition as a function of the Reynolds number and the particle Stokes number and density ratio. Important observations are as follows:

1. For Reynolds numbers between 200 and 2000, the flow over the cylinder is characterized by an unsteady wake structure and periodic asymmetric shedding of vortices in the wake. The shedding frequency or Strouhal number exhibits a relatively strong dependence on the blockage ratio, but a weak dependence on the Reynolds number. For a Reynolds number below 200, the flow becomes steady and vortex shedding is not observed, which is perhaps caused by the dissipative effect of the channel walls. For a Reynolds number above 2000, the flow tends to become turbulent. The numerical results are in agreement with those reported by previous studies.
2. Results concerning particle dynamics in an unsteady vortical flow over a cylinder indicate that all the secondary terms in the modified BBO equation are negligible compared to the steady state viscous term for particle density ratios (ε) above 20. However, they become progressively important and comparable to the steady viscous term as ε is reduced below 10. Amongst the secondary terms, the Basset history term has the largest amplitude, followed by the Saffman lift term. In addition, for a fixed Stokes number, the particle dynamics and deposition exhibit negligible dependence on particle density for $\varepsilon > 20$.
3. The particle dispersion in the presence of vortical structures in the cylinder wake exhibits a typical nonmonotonic

variation with the Stokes number. Particles with St < 0.1 behave like fluid particles, whereas those with a Stokes number in the range $0.1 <$ St < 0.5 exhibit intermediate St behavior, i.e., they are dispersed more than the fluid particles. On the other hand, particles with St > 1.0 exhibit large St behavior, i.e., they are essentially unaffected by the flow in the near wake region. In addition, while the majority of small St particles are distributed in the vortex core, the majority of intermediate St particles are distributed around the vortex periphery. These results are in accord with those reported by previous experimental and numerical studies dealing with particle dispersion in shear flows. The above observations remain qualitatively similar as the Reynolds number is varied in the range $200 <$ Re < 2000. Within this range, as Re increases the size of vortex structures in the transverse direction become larger and, consequently, the particle dispersion increases. For a Reynolds number below 200, the flow becomes steady and vortex shedding is not observed, while for Re > 2000, the flow tends to become turbulent.

4. For large particle density ratios ($\varepsilon > 20$), the particle deposition phenomena is essentially characterized by the Stokes number (St). The amount of deposition increases precipitously as the Stokes number is increased from low values (corresponding to fluid particles, i.e., St $\cong 0$ to a value of unity). For $1.0 <$ St < 3.0, the particle deposition increases relatively slowly with the Stokes number. For St > 3.0, the deposition becomes essentially independent of the Stokes number.
5. For the range of Reynolds numbers investigated, which includes both the laminar and transitional regimes, the Reynolds number (Re) has very little effect on the deposition phenomena. However, Re has a more discernible influence on particle distribution and dispersion. The particle dispersion in the unsteady wake of the cylinder is significantly increased as Re is increased from 200 to 2000.
6. For Stokes numbers >0.1, the majority of the deposition occurs on the front surface of the square cylinder. There is, however, some deposition on the rear cylinder face for very small Stokes numbers ($0.01 <$ St < 0.1). This occurs when smaller particles are picked up by the receding vortices and pulled back to the rear of the cylinder face where some are eventually deposited.

REFERENCES

Aggarwal, S. K. (1994). Relationship Between the Stokes Number and Intrinsic Frequencies in Particle-Laden Flows, *AIAA J.* 32:1322–1325.

Asgharian, B., and Godo, M. N. (1997). Transport and Deposition of Spherical Particles and Fibers in an Improved Virtual Impactor, *Aerosol Sci. Technol.* 27:499–506.

Bakkom, A. W., Crowe, C. T., Troutt, T. R., and Xu, C. (1996). Particle-Fluid Coupling Effects on Bluff Body Wakes. In *Proceeding of the ASME Fluids Engineering Division*, July, San Diego, CA, 236:273–281.

Barton, I. E. (1995). Computation of Particle Tracks over a Backward-Facing Step, *J. Aerosol Sci.* 26:887–901.

Bowen, B. D., Levine, S., and Epstein, N. (1976). Fine Particle Deposition in Laminar Flow Through a Parallel-Plate and Cylindrical Channels, *J. Colloid and Interface Sci.* 54:375–390.

Brandon, D. J. (1999). *A Numerical Investigation of Particle Deposition on a Square Cylinder Placed in a Channel Flow*, M.S. Thesis, University of Illinois at Chicago, Chicago, IL.

Chang, E., and Kailasanath, K. (1996). Simulation of Dynamics in a Confined Shear Flow, *AIAA J.* 34:1160–1166.

Chen, D. R., and Pui, D. Y. H. (1995). Numerical and Experimental Studies of Particle Deposition in a Tube with a Conical Contraction Laminar Flow Regime, *J. Aerosol Sci.* 26:563–574.

Crowe, C. T., Chung, J. N., and Trout, T. R. (1988). Particle Mixing in Free Shear Flows, *Progress in Energy and Combustion Science* 14:171–194.

Davis, R. W., Moore, E. F., and Purtell, L. P. (1984). A Numerical-Experimental Study of Confined Flow around Rectangular Cylinders, *Phys. Fluids* 27:46–59.

Duffy, G. J., and Darby, M. I. (1991). Simulated Structure of Particulate Deposition from a Model of Turbulent Gas Flow in Two Dimensions, *J. Phys. D: Appl. Phys.* 24:1665–1672.

Ghia, U., Ghia, K. N., and Shin, C. T. (1982). High-Resolutions for Incompressible Flow using the Navier-Stokes Equations and a Multigrid Method, *J. Comput. Phys.* 48:387–411.

Gupta, A. K., and Jackson, T. W. (1985). Fouling and Particulate Deposition in Practical Systems, *J. Institute of Energy* 58:103–112.

Harlow, F. H., and Welch, J. E. (1965). Numerical Calculations of Time-Dependent Viscous Incompressible Flow, *Physics of Fluids* 8:2182–2189.

Hirt, C. W., Nichols, B. D., and Romero, N. C. (1975). SOLA–A Numerical Solution Algorithm for Transient Fluid Flows, *Los Alamos National Laboratory Report*, Los Alamos, NM, April, LA-5852.

Jaluria, Y. (1988). *Computer Methods for Engineering*, Allyn & Bacon, Needham Heights, MA.

Konstandopoulos, A. G., and Rosner, D. E. (1995a). Inertial Effects on Thermophoretic Transport of Small Particles to Walls with Streamwise Curvature—I. Theory, *Int. J. Heat and Mass Transfer* 38:2305–2315.

Konstandopoulos, A. G., and Rosner, D. E. (1995b). Inertial Effects on Thermophoretic Transport of Small Particles to Walls with Streamwise Curvature—II. Experiment, *Int. J. Heat and Mass Transfer* 38:2317–2327.

Lazaro, B. J., and Lasheras, J. C. (1992). Particle Dispersion in the Developing Free Shear Layer, Part 1—Unforced Flow, *J. Fluid Mech.* 235:143–178.

Longmire, E. K., and Eaton, J. K. (1992). Structure of a Particle-Laden Round Jet, *J. Fluid Mech.* 236:217–257.

Maxey, R. M., and Riley, J. J. (1983). Equation of Motion for a Small Rigid Sphere in a Non-Uniform Flow, *Phys. Fluids* 25:883–889.

Mukhopadhyay, A., Biswas, G., and Sundararajan, T. (1993). Numerical Investigation of Confined Wakes Behind a Square Cylinder in a Channel, *Int. J. Numer. Meth. Fluids* 14:1473–1484.

Mukhopadhyay, A., Sundararajan, T., and Biswas, G. (1993). An Explicit Transient Algorithm for Predicting Incompressible Flows in Viscous Flows in Arbitrary Geometry, *Int. J. Numer. Meth. Fluids* 17:975–993.

Muyshondt, A., McFarland, A. R., and Anand, N. K. (1996). Deposition of Aerosol Particles in Contraction Fittings, *Aerosol Sci. Technol.* 24:205–216.

Odar, F., and Hamilton, W. S. (1964). Forces on a Sphere Accelerating in a Viscous Fluid, *J. Fluid Mechanics* 18:302–314.

Peng, F., and Aggarwal, S. K. (1995). A Review of Droplet Dynamics and Vaporization Modeling for Engineering Calculations, *ASME J. of Engineering for Gas Turbines and Power* 117:453–461.

Peyret, R., and Taylor, T. D. (1983). *Computational Methods for Fluid Flow*, Springer, New York, pp. 199–207.

Simons, S. (1984). Particle Deposition and Distribution in a Partially Mixed Aerosol, *J Phys. D: Appl. Phys.* 17:1797–1805.

Soh, Y. W., and Goodrich, J. W. (1988). Unsteady Solution of Incompressible Navier-Stokes Equations, *J. Comp. Phys.* 79:113–134.

Stratmann, F., Fissan, H., and Petersen, T. W. (1988). Particle Deposition onto a Flat Surface from a Point Particle Source, *American Chemical Society* 31:39–41.

Suh, Y. J., and Kim, S. S. (1996). Effect of Obstructions on the Particle Collection Efficiency in a Two-Stage Electrostatic Precipitator, *J. Aerosol Sci.* 27:61–74.

Thatcher, T. L., and Nazaroff, W. W. (1997). Effect of Small-Scale Obstructions and Surface Textures on Particle Deposition from Natural Convection, *Aerosol Sci. Technol.* 27:709–725.

Tu, J. Y., and Fletcher, C. A. J. (1995). Numerical Computation of Turbulent Gas-Solid Particle Flow in a 90° Bend, *AIChE J.* 41:2187–2197.

Uthuppan, J., Aggarwal, S. K., Grinstein, F. F., and Kailasanath, K. (1994). Particle Dispersion in a Transitional Axisymmetric Jet: A Numerical Simulation, *AIAA J.* 32:2004–2014.

Vasak, F., Bowen, B. D., Chen, C.Y., Kastanek, F., and Epstein, N. (1995). Fine Particle Deposition in Laminar and Turbulent Flows, *The Canadian Journal of Chemical Engineering* 73:785–791.

Viatistas, N. T. (1992). Effect of Adhesion Time on Particle Deposition: Reentrainment and Rolling, *American Chemical Society* 31:1549–1554.

Wang, Q., and Squires, K. D. (1996). Large Eddy Simulation of Particle Deposition in a Vertical Turbulent Channel Flow, *Int. J. Multiphase Flow* 22:667–683.

Ye, Y., and Pui, D. Y. H. (1990). Particle Deposition in a Tube with an Abrupt Contraction, *J. Aerosol Sci.* 21:29–40.

Yu, G., Zhang, Z., and Lessmann, R. (1996). Computer Simulation of the Flow Field and Particle Deposition by Diffusion in a 3-D Human Airway Bifurcation, *Aerosol Sci. Technol.* 25:338–352.

Zhang, L., Asgharian, B., and Anjilvel, S. (1997). Internal Deposition of Particles in the Human Upper Airway Bifurcations, *Aerosol Sci. Technol.* 26:97–110.